Environmental Science and Ecotechnology 22 (2024) 100455

Contents lists available at ScienceDirect

Environmental Science and Ecotechnology

journal homepage: www.journals.elsevier.com/environmental-science-and-ecotechnology/

Original Research

Optimizing UVA and UVC synergy for effective control of harmful cyanobacterial blooms

Yinjie Zhu [a, b, c, d, 1], Jian Ding [a, b, c, 1], Xiaoxiong Wang [e], Xuejian Wang [a, b, c], Huansheng Cao [f], Fei Teng [a, b, c, d], Shishi Yao [a, b, c, d], Zhiru Lin [a, b, c, d], Yuelu Jiang [e], Yi Tao [a, b, c, d, *]

[a] Guangdong Provincial Engineering Research Center for Urban Water Recycling and Environmental Safety, Tsinghua Shenzhen International Graduate School, Tsinghua University, Shenzhen, Guangdong, 518055, China
[b] Key Laboratory of Microorganism Application and Risk Control (MARC) of Shenzhen, Tsinghua Shenzhen International Graduate School, Tsinghua University, Shenzhen, Guangdong, 518055, China
[c] Shenzhen Key Laboratory of Ecological Remediation and Carbon Sequestration, Tsinghua Shenzhen International Graduate School, Tsinghua University, Shenzhen, Guangdong, 518055, China
[d] Tsinghua University-Kunming Joint Research Center for Dianchi Plateau Lake, Tsinghua University, Beijing, 100084, China
[e] Institute for Ocean Engineering, Tsinghua Shenzhen International Graduate School, Tsinghua University, Shenzhen, 518055, China
[f] Division of Natural and Applied Sciences, Duke Kunshan University, Kunshan, Jiangsu, 215300, China

ARTICLE INFO

Article history:
Received 18 February 2024
Received in revised form
6 July 2024
Accepted 7 July 2024

Keywords:
Cyanobacterial bloom
Ultraviolet irradiation
Photosynthetic damage
DNA damage/repair
Regulated cell death

ABSTRACT

Harmful cyanobacterial blooms (HCBs) pose a global ecological threat. Ultraviolet C (UVC) irradiation at 254 nm is a promising method for controlling cyanobacterial proliferation, but the growth suppression is temporary. Resuscitation remains a challenge with UVC application, necessitating alternative strategies for lethal effects. Here, we show synergistic inhibition of *Microcystis aeruginosa* using ultraviolet A (UVA) pre-irradiation before UVC. We find that low-dosage UVA pre-irradiation (1.5 J cm^{-2}) combined with UVC (0.085 J cm^{-2}) reduces 85% more cell densities compared to UVC alone (0.085 J cm^{-2}) and triggers *mazEF*-mediated regulated cell death (RCD), which led to cell lysis, while high-dosage UVA pre-irradiations (7.5 and 14.7 J cm^{-2}) increase cell densities by 75–155%. Our oxygen evolution tests and transcriptomic analysis indicate that UVA pre-irradiation damages photosystem I (PSI) and, when combined with UVC-induced PSII damage, synergistically inhibits photosynthesis. However, higher UVA dosages activate the SOS response, facilitating the repair of UVC-induced DNA damage. This study highlights the impact of UVA pre-irradiation on UVC suppression of cyanobacteria and proposes a practical strategy for improved HCBs control.

1. Introduction

Harmful cyanobacterial blooms (HCBs) have been a serious global issue for decades, posing threats to drinking water safety and the diversity of aquatic ecosystems [1–4] due to the biosynthesis and release of cyanotoxins and taste and odor compounds [5–10]. The outbreak of HCBs has become even worse in the last decade owing to global warming [11]. Various methods have been investigated and applied to control the explosion of HCBs, including ultraviolet [12,13], ultrasonication [14], algaecides [15–19], and photocatalysis [20]. In addition, combined strategies coupling damages on different intracellular compartments for synergistic effects have been widely investigated, opening avenues for advanced approaches for HCB control [21–24].

Ultraviolet C (UVC) irradiation at 254 nm has been recommended as an efficient and environmentally friendly approach to cyanobacterial growth control [12]. UVC causes damage to photosystem II (PSII) via direct absorption by plastoquinone [25] and indirect suppression of photosynthetic genes [26] due to deoxyribonucleic acid (DNA) damage [13]. These lead to electron leakage and energy accumulation in reaction centers [27], rising reactive oxygen species (ROS) in microalgal cells [27,28], and eventually

* Corresponding author.
E-mail address: tao.yi@sz.tsinghua.edu.cn (Y. Tao).
[1] The authors contributed equally to the work.

https://doi.org/10.1016/j.ese.2024.100455

inducing cyanobacterial regulated cell death (RCD) [29]. Like UVC, 365-nm ultraviolet A (UVA) irradiation, the main UV component in solar light reaching the Earth's surface [30], can also inactivate bacterial cells [31,32]. UVA exposure causes negligible direct damage to DNA [33,34] but produces intracellular ROS [35–37]. Moreover, the collapse of cellular iron-sulfur (Fe–S) clusters and catalase inactivation induced by UVA irradiation have been reported [33,36–38], contributing to lethal Fenton reactions in cells. Thus, the different mechanisms of UVA and UVC lethality and the easy access to UVA have inspired attempts to combine both to enhance UVC disinfection efficiency. This has been proven effective in experiments with *Escherichia coli*, *Enterococcus faecalis,* and bacteriophage MS2 [34,39–42]. In contrast, information regarding the control of photosynthetic organisms based on UVA and attempts to combine UVA and UVC in HCB control is limited [43–46].

However, caution must be raised, as UVA may exert a dual role when combined with UVC. UVA has been reported to activate the DNA repair system by upregulating the SOS response genes, particularly gene *recA* [38], and thus may compromise UVC suppression. Therefore, we hypothesized that there is a tradeoff between DNA damage repair provided by UVA and synergistic inhibition by UVA–UVC treatment. In addition, the dual effects of UVA pre-irradiation may modulate cell fates toward growth recovery or cell death. Cyclobutene pyrimidine dimers [13] and oxidative damage [37] caused by UVC and UVA, respectively, finally lead to cellular RCD if irreparable [47]. Among various RCD modes [48–51], only apoptosis, or apoptosis-like death (ALD) in prokaryotes, has been extensively investigated in *Microcystis* strains in recent decades [29,52]. However, the widely existing prokaryotic *mazEF* system [53] has yet to be studied in *M. aeruginosa*. The *mazEF* system is composed of an antitoxin, mazE, and a toxin, mazF. Once activated, the antitoxin mazE is degraded, and the toxin mazF is active in cleaving messenger ribonucleic acid (mRNA), blocking protein translation, and finally leading to RCD [54]. Aside from DNA damage, many stresses have been reported to initiate *mazEF*-mediated RCD, including oxidative stress [55]. Increasing evidence has even revealed the regulating role of *mazEF*-mediated RCD in delaying ALD in bacteria [54,56–58].

This study investigated the effects of UVA–UVC sequential irradiation on a typical cyanobacteria species of *M. aeruginosa*. This work aimed to assess how the pre-irradiation of UVA (365 nm) influenced UVC (254 nm) suppression in *M. aeruginosa* cells. In addition, we aimed to demonstrate the intertwining of *mazEF*-mediated RCD and ALD in *M. aeruginosa* cells exposed to sequential UVA–UVC irradiation. By analyzing photosynthetic parameters, including photosynthetic oxygen evolution, effective quantum yields of PSII and photosystem I (PSI), and expression profiles of photosynthetic genes, it was found that UVA and UVC acted independently on PSI and PSII, respectively. Thus, the combination of UVA and UVC synergistically damaged the photosynthetic electron transport chain (ETC). However, with increased UVA dosages, synergy was muted, and cell recovery was realized because UVA at higher dosages provided efficient DNA repair. Furthermore, the results obtained at the cellular, molecular, and transcriptomic levels indicated that *M. aeruginosa* cells were induced into different levels of *mazEF* stress and underwent either RCD or recovery based on UVA dosages. It validates the potential of *mazEF* stress induction by UVA pre-irradiation in regulating cyanobacterial physiological states.

2. Materials and methods

2.1. Microalgal cultivation and irradiation experiments

Axenic *M. aeruginosa* FACHB905 was purchased from the FACHB-Collection at the Institute of Hydrobiology, Chinese Academy of Science, Wuhan, China, and incubated in sterile BG11 medium (Supplementary Material Tables S1 and S2) at 25 ± 1 °C under an irradiance of 1500 lx (measured with HOBO MX2202, USA) provided by four cool white fluorescent lamps (6.5 W for each, Philips, Shanghai, China) in an incubator (Yiheng, Shanghai, China), with a 12/12 h light/dark irradiation cycle [29].

Microalgae during their exponential growth phase were harvested and diluted to around 1.4×10^6 cells mL^{-1} with sterile BG11 medium before experiments. An ultraviolet light-emitting diode (UV-LED) device (2W, HONGLIZHIHUI BYTECH, Guangzhou, China) emitting 365 nm UVA and a collimated beam apparatus equipped with two low-pressure lamps (75 W, Philips, Shanghai, China) emitting 254 nm UVC were used to accomplish UVA pre-irradiation and subsequent UVC irradiation of *M. aeruginosa* (Supplementary Material Fig. S1). The absorbance of *M. aeruginosa* at 365 nm was measured and compared with that at 680 nm using a multimode microplate reader (SpectraMax i3; Molecular Devices, CA, USA). The results demonstrated that *M. aeruginosa* cells could absorb UVA comparable to 680 nm light (Supplementary Material Fig. S2).

Briefly, for each dosage of UVA irradiation, a microalgal suspension of 100 mL was irradiated in glass Petri dishes with a diameter of 100 mm. The UVA incident fluence rate (Supplementary Material Fig. S3) was measured using the potassium ferrioxalate actinometry method according to previous works [59,60] and corrected with the water factor (WF) to calculate the average fluence rate (Supplementary Material Text S1, Table S3) [61,62]. The average fluence rate of UVA was maintained at 2.73 mW cm^{-2}. Thus, by varying the exposure time to 9, 45, and 90 min, UVA dosages of 1.5, 7.5, and 14.7 J cm^{-2} were determined, respectively. After UVA pre-irradiation, suspensions of 100 mL each were irradiated with 0.085 J cm^{-2} UVC (average fluence rate = 1.24 mW cm^{-2}, 68 s irradiation) in 90 mm Petri dishes in a collimated beam apparatus equipped with two low-pressure lamps (75 W) emitting UVC at 254 nm. The UVC incident fluence rate at the suspension surface was measured using a UV sensor (RM12; Dr. Grobel Elektronik, Germany) and also corrected with the WF to calculate the average fluence rate (Supplementary Material Table S3). Suspensions without both UVA and UVC irradiation were set as controls.

In addition, suspensions irradiated with UVA alone (7.5 J cm^{-2}) and UVC alone (0.085 J cm^{-2}) were also selected for comparison. In our preliminary experiments, 7.5 J cm^{-2} UVA negligibly influenced microalgal growth and equivalently influenced the effects of UVC to 14.7 J cm^{-2}. Thus, we chose 7.5 J cm^{-2} for individual UVA irradiation due to the relatively shorter irradiation time. A magnetic stirrer was used in each dish to homogenize the suspension and ensure uniform irradiation. After treatment, suspensions of 100 mL each were transferred into 250 mL Erlenmeyer flasks and incubated under the same conditions mentioned above. Samples were analyzed immediately after UVC irradiation (2 h, corresponding to 0.1 d) and on 1, 2, 3, 5, 7, 10, and 14 days afterward. Three replicates were conducted for each treatment. The detailed irradiation methods are shown in Fig. 1. For convenience, the labels of each group are listed in Supplementary Material Table S4.

2.2. Microcystin-LR quantification

Both total and extracellular microcystin-LR (MC-LR) produced by *M. aeruginosa* were determined and quantified using ultra-high performance liquid chromatography (UPLC) (Nexera X2, LC-30AD; Shimadzu, Kyoto, Japan) coupled with tandem mass chromatography (MS)/MS (QTRAP® 6500+; AB Sciex, CA, USA) with a reference MC-LR from Sigma-Aldrich (MO, USA) (Supplementary Material Fig. S4). For extracellular MC-LR quantification, 0.45 μm Polyvinylidene Fluoride films (JET Inc., Shanghai, China) were used

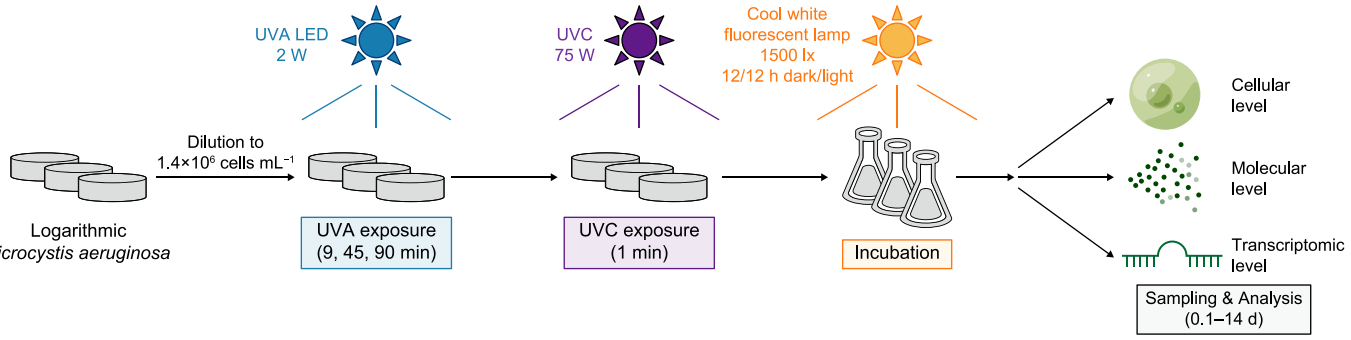

Fig. 1. Schematic illustration of the experimental setup. The UVA LED and UVC wavelengths were 365 and 254 nm, respectively. Sampling and analysis were performed on 0.1, 1, 2, 3, 5, 7, 10, and 14 days after UV irradiation.

to collect the filtrate for further analysis. The concentration of intracellular MC-LR was calculated as the difference between the total and extracellular MC-LR concentrations (equation (1)). The MC-LR quota was calculated as intracellular MC-LR divided by viable cell density (equation (2)). The parameters for LC-MS/MS analysis of MC-LR are listed in Supplementary Material Table S5.

$$Intracellular\ MC-LR = Total\ MC-LR - Extracellular\ MC-LR \quad (1)$$

$$MC-LR\ quota = \frac{Intracellular\ MC-LR}{Viable\ cell\ density} \quad (2)$$

2.3. Measurement of photosynthesis and energy state

The effective quantum yields of PSII and PSI, *Y*(II) and *Y*(I), were determined using the phytoplankton pulse-amplitude-modulated fluorometer (PHYTO-PAM; Walz, Effeltrich, Germany) [29] and dual-pulse-amplitude-modulation (Dual-PAM) (Walz, Effeltrich, Germany), respectively, according to equation (3) [15].

$$Y = \frac{(F_m' - F_0')}{F_m'} \quad (3)$$

where Y is the effective quantum yield; F_m' is the light-adapted maximal Chl a fluorescence measured when all the reaction centers are closed; F_0' is the light-adapted minimal Chl a fluorescence measured when all the reaction centers are open.

Photosynthetic oxygen evolution rates were measured with an oxygen fluorescent electrode setup (YZQ-201A; YZQ Technology Co., Beijing, China) by recording the time-scale evolution of dissolved oxygen. Briefly, *Microcystis aeruginosa* cells were centrifuged at 5000 rpm for 15 min, washed three times with phosphate buffer saline (PBS), resuspended in a sterile BG11 medium, and injected into the setup chamber equipped with a light-emitting diode (LED) lamp (RGB, 800 μmol photons $cm^{-1}\ s^{-1}$) and a magnetic stirrer (40 rpm). A 15-min dark adaptation was conducted, followed by determining the dark respiration when cells were exposed to darkness and photosynthetic oxygen evolution rates when exposed to light. The types and concentrations of reagents utilized to measure the activities of different sections of the whole photosynthetic ETC are listed in Supplementary Material Table S6. PSII activities were identified as oxygen production with H_2O as the electron donor and *para*-benzoquinone (*p*-BQ) as the acceptor. PSI activities were measured as oxygen consumption, with 3-(3′,4′-dichlorophenyl)-1,1-dimethylurea (DCMU) as PSII inhibitor, ascorbic acid-reduced 2,6-dichlorophenol indophenol ($DCPIPH_2$) as electron donor, and methyl viologen (MV) as acceptor (Supplementary Material Fig. S5) [15,63,64]. Measurement was conducted under 24 °C. Note that 24 °C could inhibit algal respiration (Supplementary Material Fig. S6) to avoid interference from cytochrome *c* oxidase (COX), which conveys electrons from photosynthetic ETC to oxygen.

The adenosine triphosphate (ATP) level of the cells was measured with the CellTiter-Glo® Luminescent Cell Viability Assay Kit (Promega, WA, USA) [29]. Briefly, 100 μL working reagent was mixed with an aliquot of 100 μL sample in each well of a 96-well plate (Corning, NY, USA). The mixture was incubated for 15 min in the dark at room temperature, followed by luminescence intensity measurement on a multimode microplate reader (SpectraMax i3; Molecular Devices, CA, USA). The results were normalized and expressed relative to the control [29].

2.4. Flow cytometric analysis

A flow cytometer (FACS-Calibur; Beckton Dickinson, NJ, USA) equipped with lasers of 488 and 635 nm and signal acquisition channels of FSC, SSC, FL1, FL2, FL3, and FL4 was used to investigate cell density, pigment contents, membrane integrity, oxidative stress, and ALD hallmarks (i.e., membrane potential, caspase-3-like enzyme activity, phosphatidylserine externalization, and terminal deoxynucleotidyl transferase dUTP nick-end labeling [TUNEL] positive rate). Details are demonstrated in Supplementary Material Text S2.

2.5. Observation of morphology and ultrastructure

The morphology and ultrastructure of microalgal cells were detected using a field emission scanning electron microscope (FE-SEM, SU8010; Hitachi, Tokyo, Japan) and transmission electron microscope (TEM) (Tecnai G2, FEI, USA) [29], respectively, with modifications. For morphological observation, 10 mL microalgal samples were taken from each group and centrifuged at 9,000 rpm for 5 min. The supernatant was discarded, and the microalgal pellets were fixed in 2.5% glutaraldehyde overnight at 4 °C. Samples were centrifuged at 10,000 rpm for 10 min and washed three times with PBS buffer. Afterward, graded dehydration was carried out sequentially in 50%, 70%, 80%, 90%, and 100% (v/v) ethanol (Aladdin, Shanghai, China), 50% (v/v) ethanol in *tert*-butyl alcohol (Aladdin, Shanghai, China), and 100% *tert*-butyl alcohol for 10 min each time. Fresh *tert*-butyl alcohol was added to the samples and kept under −20 °C until lyophilization (FDU-1110; EYELA, China). Finally, the samples were sputtered with Au using ion sputtering (MC1000; Hitachi, Japan) and observed with FE-SEM (SU8010; Hitachi, Tokyo, Japan).

For ultrastructural observation, a volume of 10 mL samples was harvested by centrifugation at 9,000 rpm for 5 min. The

supernatant was discarded, and pellets were washed three times with PBS, fixed in 2.5% glutaraldehyde overnight at 4 °C, buffered in PBS, post-fixed in 2% osmium tetroxide for 8 h, dehydrated in graded ethanol series, and finally embedded in epoxy resin Epon812 (Sigma-Aldrich, MO, USA). Ultrathin sections (70–90 nm) were prepared using an ultramicrotome (EM UC7; Leica, Germany), stained with uranyl acetate and lead citrate for 10 min, and observed with TEM (Tecnai G2; FEI, USA).

2.6. Transcriptomic analysis

Microcystis aeruginosa cells in all groups were harvested on the 2nd and 10th days for ribonucleic acid (RNA) extraction, processing, sequencing, and transcriptomic analysis (i.e., Venn diagrams analysis, volcano plots analysis, gene ontology [GO], Kyoto Encyclopedia of Genes and Genomes [KEGG] analysis, and heatmap clustering). Details are described in Supplementary Material Text S3. The processed clean reads were submitted to the National Center of Biotechnology Information Sequence Read Archive (accession number: PRJNA822848).

2.7. Statistical analysis

All treatments were conducted in triplicate, presenting the results as mean ± SD. Data processing and analysis were conducted using Origin 2018c software (OriginLab, MA, USA). Statistical differences between groups were analyzed using one-way analysis of variance (ANOVA) followed by Tukey's test. The median effective time (ET_{50}, Supplementary Material Table S7) was calculated using first-order fitting to evaluate the sensitivity of *M. aeruginosa* to different irradiation patterns. Lower ET_{50} values indicate the more potent effects of irradiation in *M. aeruginosa* cells and vice versa.

3. Results and discussion

3.1. Physiological responses to UV irradiation

A bidirectional impact of UVA pre-irradiation on UVC-induced suppression effects at different UVA dosages was observed. Pre-irradiation at a low UVA dosage (1.5 J cm^{-2}) enhanced UVC-induced growth suppression effects on *M. aeruginosa* cells. In contrast, pre-irradiation at higher UVA dosages (7.5 and 14.7 J cm^{-2}) compromised the growth suppression effects (Fig. 2). Specifically, for the mono UVC group at [0, 0.085] and UVA/UVC groups at [1.5, 0.085], [7.5, 0.085], and [14.7, 0.085], microalgal growth was significantly suppressed ($p < 0.01$) with growth inhibition rates of 95%, 96%, 93%, and 93%, respectively, on the 14th day (Fig. 2a). Prominently, from the 10th to the 14th day, significant 50–60% increases in cell densities were observed when 7.5 and 14.7 J cm^{-2} UVA were pre-irradiated ($p < 0.05$). However, for the mono UVC group and the UVA/UVC group at [1.5, 0.085], insignificant changes were detected ($p > 0.05$). The lowest cell density (1.67×10^6 cells mL^{-1}) was observed in the UVA/UVC group at [1.5, 0.085] on the 14th day. In contrast, the UVA/UVC groups with higher UVA dosages ([7.5, 0.085] and [14.7, 0.085]) exhibited 36–41% higher cell densities than the mono UVC group.

The lethal effects represented by membrane permeabilization indicated the bidirectional impacts of UVA pre-irradiation, as shown in Fig. 2b. UVC irradiation alone induced a remarkable increase in the percentages of cells with permeabilized membranes, which reached 81% on the 14th day, with an ET_{50} of 8.1 d (Supplementary Material Table S7). The pre-irradiation of UVA at different dosages aggravated the membrane permeabilization before the 10th day, with the lowest 1.5 J cm^{-2} constantly causing the severest integrity loss, indicating a synergy between UVA and UVC in damaging cell membranes. However, this synergy seemed saturated at 1.5 J cm^{-2} UVA, as increasing the UVA dosages did not necessarily further permeabilize the membranes. Afterward, a divergence appeared. In detail, the UVA/UVC group at [1.5, 0.085] demonstrated the highest value at 96% on the 14th day and the lowest ET_{50} (6.1 d), suggesting that UVA pre-irradiation at 1.5 J cm^{-2} markedly enhanced the lethal effects of UVC irradiation. Moreover, cells of the UVA/UVC groups at [7.5, 0.085] ($ET_{50} = 6.6$ d) and [14.7, 0.085] ($ET_{50} = 7.4$ d) on the 14th day exhibited 12% and 26% lower percentages ($p < 0.05$) than those of the UVC group, indicating that UVA pre-irradiation at 7.5 J cm^{-2} and above alleviated the lethal effects of UVC.

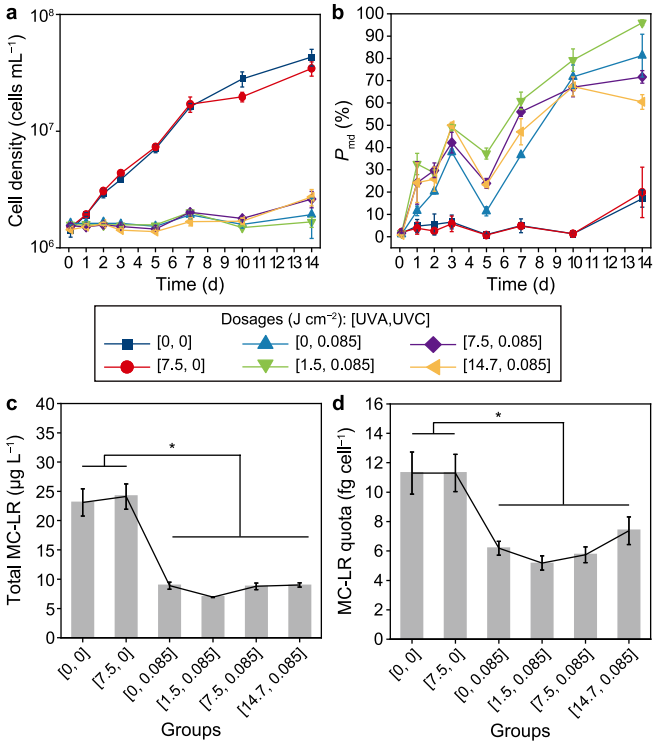

Fig. 2. Physiological responses of *Microcystis aeruginosa* to UV irradiation. **a**, Time-scale total cell density changes under 1500 lx at 25 ± 1 °C with a 12/12 h dark/light cycle. **b**, Time-scale changes of the percentage of cells with permeabilized membranes under 1500 lx at 25 ± 1 °C with a 12/12 h dark/light cycle. **c**, Total microcystin-LR. **d**, Microcystin-LR cellular quota on the 7th day of post-incubation. Asterisks indicate significant differences at $p < 0.05$. The error bar represents the standard deviation from the three biological replicates.

The results of TEM (Supplementary Material Fig. S7) and SEM (Supplementary Material Fig. S8) demonstrated that UVA pre-irradiation at 1.5 J cm^{-2} further aggravated cellular structural collapse upon UVC. In contrast, pre-irradiation at higher UVA dosages helped relieve the pressure. Cells of the mono UVC and UVA/UVC groups at [1.5, 0.085] (Supplementary Material Figs. S7c and d) experienced severe deformation of cell membranes, plasmolysis, accumulation of polyphosphate bodies (PPBs), and collapse of thylakoid membranes. Moreover, more PPBs and slight cytoplasmic vacuolization appeared only in the UVA/UVC group at [1.5, 0.085] (Supplementary Material Fig. S7d). As the dosages of UVA pre-irradiation increased, less plasmolysis and PPBs were observed in the microalgal cells compared with those in cells of the mono UVC group at [0, 0.085] and the UVA/UVC group at [1.5, 0.085] (Supplementary Material Figs. S7e and f). The results of SEM (Supplementary Material Fig. S8) and membrane damage (Fig. 2b) corresponded with the ultrastructural damage.

Results of MC-LR showed that UVA pre-irradiation at 1.5 J cm^{-2} further enhanced the inhibition effects on toxin synthesis upon UVC. Total, extracellular, and intracellular MC-LR of the mono UVC group and all the UVA/UVC groups were consistently inhibited compared with the control group within 7 d (Fig. 2c; Supplementary Material Figs. S9a–c). As indicated by the cellular quota in the mono UVC group and all the UVA/UVC groups, biosynthesis was consistently suppressed within 7 d (Fig. 2d; Supplementary Material Fig. S9d). Then, slight increases in MC-LR quota values were observed in all the UVA/UVC groups on the 10th and 14th day (Supplementary Material Fig. S9d). The transcriptomic results also indicated that MC-LR biosynthesis was significantly inhibited in the mono UVC and all the UVA/UVC groups within two days post-exposure incubation, while it recovered to just slightly lower than the control on the 10th day (Supplementary Material Fig. S9e, Table S8). This corresponded to a ~30% suppression of MC-LR quota values compared with control within 10 days (Supplementary Material Fig. S9d). However, 2–5 times higher concentrations of extracellular MC-LR compared with control were detected on the 10th and 14th day in these four groups, possibly due to significant enhancement of membrane permeabilization compared with the control ($p < 0.05$) (Fig. 2b), similar to a previous report on plasma-induced toxin release in *M. aeruginosa* [65]. Moreover, a low UVA dosage (1.5 J cm^{-2}) did not enhance the risk of MC-LR release compared with the mono UVC group. However, more substantial membrane damage was observed in this group (Fig. 2b). The above results indicated that although a low UVA dosage enhanced UVC lethality, the toxin biosynthesis potential was extensively and most effectively inhibited (Fig. 2d).

3.2. Synergistic photosynthetic damage induced by sequential UVA–UVC irradiation

UVA and UVC caused independent damage to photosystems I and II, respectively, and thus synergistically compromised *M. aeruginosa* photosynthesis when irradiated sequentially. Oxygen evolution tests (Supplementary Material Fig. S5) indicated that mono UVA treatment resulted in a ~30% decrease in the PSI ETC rate. In comparison, mono UVC treatment led to a ~75% decrease in the PSII ETC rate (Fig. 3a). The combination of the two wavelengths of UV failed to aggravate the damage to these separate photosynthetic apparatuses, confirming the independent damage pathways caused by UVA and UVC. The Dual-PAM test (Fig. 3b and c) revealed that UVA and UVC caused prominent decreases in PSI and PSII quantum yields, respectively. The GO enrichment analysis (Supplementary Material Fig. S10) confirmed the above results.

Variations in the *Y*(II) values measured using PHYTO-PAM also demonstrated the synergism of UVA–UVC exposure and the bidirectional impacts of UVA pre-irradiation, as shown in Fig. 3d and S Supplementary Material Fig. 11a. The *Y*(II) value of the mono UVC group declined by 20% within 0.1 d post-incubation, decreased sharply to 0.02 within 2 d ($ET_{50} = 0.6$ d) and gradually recovered after the 7th day. By contrast, the *Y*(II) of the mono UVA group dropped immediately (0.1 d) to 0.3, 10% lower than that of the UVC group ($p < 0.01$), and then quickly returned to the control level within 2 d, indicating substantial but temporary UVA damage to the photosynthesis of *M. aeruginosa* cells. *Y*(II) values of all the UVA/UVC groups drastically dropped below 0.1 within 0.1 d, significantly and synergistically lower than the mono UVC and UVA groups ($p < 0.01$, $ET_{50} < 0.1$ d; Supplementary Material Table S7; Fig. 3d). Moreover, UVA pre-irradiation followed by UVC resulted in a significant 80% decline in the ETC rate of the whole photosynthetic apparatuses (Fig. 3a). During post-incubation (Supplementary Material Fig. S11a), the *Y*(II) values of all the UVA/UVC groups recovered since the 5th day with similar patterns to the mono UVC group. In detail, a smaller UVA dosage (1.5 J cm^{-2}) postponed the recovery of *Y*(II). This resulted in a lower *Y*(II) value than the mono UVC group, while the larger UVA dosages (7.5 J cm^{-2} and above) marked accelerated recovery back to the control level.

The transcriptomic data of photosynthetic genes for PSII, PSI, and phycobilisome indicated that UVA pre-irradiation at 7.5 J cm^{-2} and above alleviated UVC-induced damage to genes encoding the photosynthetic system. Cellular photosynthesis experienced a process of damage (2nd day) followed by recovery (10th day) (Supplementary Material Fig. S11b, Table S9). On the 2nd day, all five PSI genes (*psaB*, C789_RS21395; *psaA*, C789_RS21390; *psaC*, C789_RS03195; *psaK*, C789_RS04160, C789_RS21660) and several PSII genes (*psb28*, C789_RS15295; *psb27*, C789_RS00160; *psbP*, C789_RS0022) were significantly downregulated in the mono UVA group (Supplementary Material Table S9). By contrast, UVC and UVA/UVC irradiation downregulated all the PS genes, and as UVA dosages increased over 7.5 J cm^{-2}, the downregulation level was markedly reduced (Supplementary Material Table S9). On the 10th day, several photosynthetic genes were upregulated in the mono UVC and all UVA/UVC groups. Among these, increasing

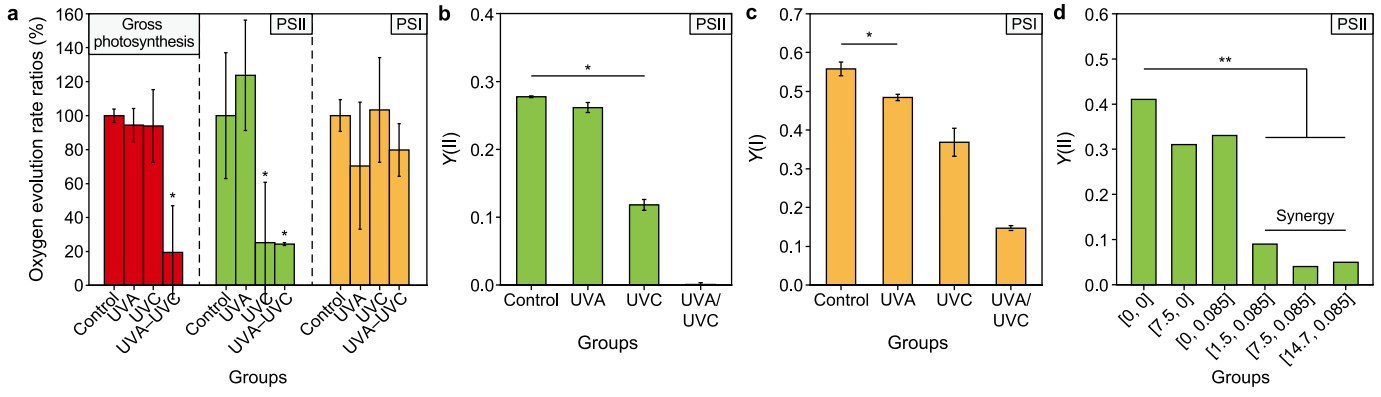

Fig. 3. Synergistic photosynthetic damage caused by sequential UVA and UVC irradiation. **a**, Oxygen evolution rates of algal solutions at 2 h after UVA and UVC irradiation. Oxygen evolution rates were measured under 800 μmol photons cm^{-1} s^{-1} and expressed as (irradiated/control groups) %. **b**–**c**, The effective quantum yields of PSII (**b**) and PSI (**c**) of *Microcystis aeruginosa* cells were measured using Dual-PAM at 2 h after UV irradiation. **d**, The effective quantum yields of PSII of *M. aeruginosa* cells at 2 h after UV irradiation were measured using PHYTO-PAM. UVA and UVC independently target PSI and PSII, respectively. The sequential irradiation of UVA and UVC blocked all electron transport chains. In panels **a**, **b**, and **c**, the UVA and UVC dosages were 7.5 and 0.085 J cm^{-2}, respectively. Asterisks indicate significant differences with * at $p < 0.05$ and ** at $p < 0.01$. The error bar represents the standard deviation from the three biological replicates.

upregulation levels of PSI genes while downregulation of PSII genes was observed as UVA dosages increased compared to the mono UVC group (Supplementary Material Table S9).

Along with photosynthetic collapse, ATP generation was blocked at the biochemical (Supplementary Material Fig. S12a) and transcriptional (Supplementary Material Fig. S12b, Table S10) levels. Along with the ATP shortage, the Calvin cycle genes were downregulated (Supplementary Material Fig. S13, Table S11). However, *Y*(II) recovery after the 10th day corresponded to increases in ATP levels and upregulation of ATP synthase (Supplementary Material Fig. S12) and Calvin cycle genes (Supplementary Material Fig. S13).

The results obtained from oxygen evolution tests, PHYTO-PAM, Dual-PAM, and transcriptome analysis concluded that UVA and UVC independently damaged PSI and PSII, respectively. Thus, the combination of UVA and UVC synergistically compromised the photosynthetic ETCs (Supplementary Material Fig. S14). This would impose pressure on the overall metabolism of *M. aeruginosa* cells.

3.3. Oxidative stress and mazEF stress induced by UV irradiation

The synergism and the bidirectional impacts in photosynthetic damage caused by sequential UVA–UVC irradiation gave rise to gradual elevation patterns and bidirectional effects on intracellular oxidative stress (Fig. 4a–c; Supplementary Material Fig. S15), which finally led to varying *mazEF* stress levels in *M. aeruginosa* cells.

Intracellular ROS showed that UVA pre-irradiation at 1.5 J cm^{-2} induced the highest oxidative stress level and the most severe DNA damage. Intracellular ROS in the mono UVC group and all the UVA/UVC groups fluctuated above the control level within the initial five days, then increased and peaked on the 7th day, and remained stable at ~3-fold of control afterward (Supplementary Material Fig. S15a). Furthermore, the superoxide anion radical ($O_2^{\cdot-}$) (Fig. 4a) increased on the 5th day and peaked on the 10th day at 6–12 fold of the control in these four groups. For hydroxyl radical (•OH) (Fig. 4c), it increased on the 7th day and peaked on the 10th day at 1–3 fold of the control in these four groups. Both radicals remained since then in the order of UVA/UVC group at [1.5, 0.085] > mono UVC group > UVA/UVC group at [7.5, 0.085] ≈ UVA/UVC group at [14.7, 0.085]. The lagged increase of intracellular •OH compared with that of intracellular $O_2^{\cdot-}$ could be explained by the rise of intracellular hydrogen peroxide (H_2O_2) since the 6th day (Fig. 4b). Moreover, the level of intracellular •OH was equivalent to that of intracellular ROS, indicating the prevailing •OH stress inside cells. This would cause DNA damage and, if beyond repair, would finally lead to RCD. As the TUNEL positive rate indicated, the DNA double-strand break increased from the 2nd to the 7th day (Supplementary Material Fig. S16). It peaked on the 7th day at 2.13-fold in the mono UVC group [0, 0.085] and 2.66, 2.07, and 1.81-fold

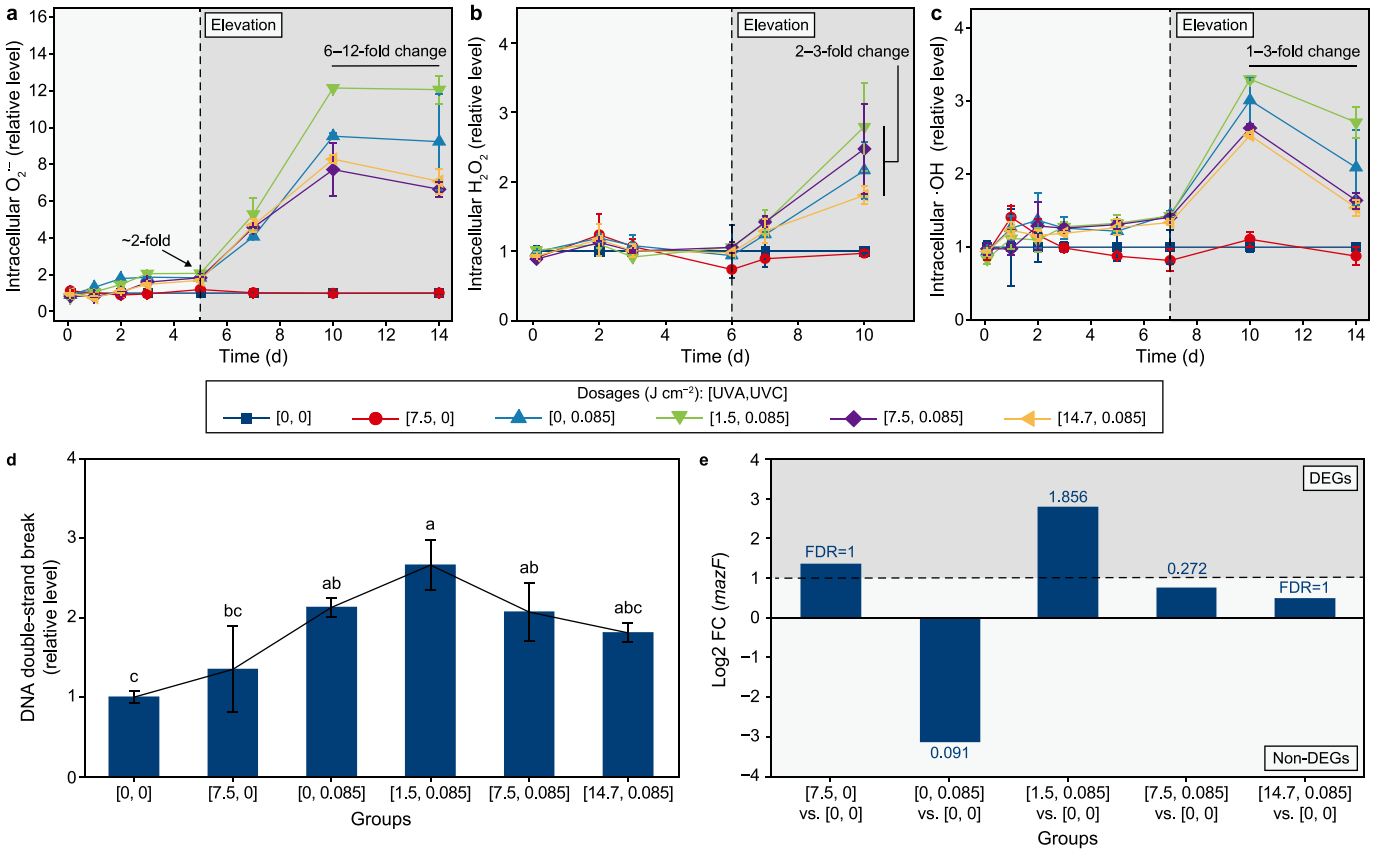

Fig. 4. Oxidative and *mazEF* stress induced by UV irradiation of *Microcystis aeruginosa* cells. **a**–**c**, Time-scale changes in intracellular oxidative stress as indicated by superoxide anion radicals (**a**), hydrogen peroxide (**b**), and hydroxyl radicals (**c**) in *M. aeruginosa* cells under 1500 lx at 25 ± 1 °C with a 12/12 h dark/light cycle. Light grey indicates negligible changes of, while dark grey suggests significant elevation of ROS compared with that of the control. **d**, DNA double-strand break on the 7th day after UV irradiation, as indicated by the TUNEL positive rates. **e**, Log2FC of gene *mazF* on the 10th day after UV irradiation. The data above columns represent −log10(FDR) of gene expression changes, and genes with −log10(FDR) above 1.301 are considered differentially expressed genes (DEGs). Light grey indicates Non-DEGs, while dark grey suggests DEGs. In general, synergistic damage to the whole photosynthetic ETC resulted in the generation and conversion of ROS in *M. aeruginosa* cells. The ROS burst, DNA double-strand break, and *mazEF* stress proceeded chronologically within 10 d. Different letters indicate significant differences between the groups. The error bar represents the standard deviation from the three biological replicates.

in the UVA/UVC groups at [1.5, 0.085], [7.5, 0.085], and [14.7, 0.085], respectively (Fig. 4d).

In response to ROS burst, two oxidative stress response genes (*grxC*, C789_RS01515; and *cmpR*, C789_RS14990) were significantly upregulated in the mono UVA group on the 2nd day (Supplementary Material Figs. S15b and S17, Table S12). Half of the genes were upregulated in the mono UVC group [0, 0.085] and all UVA/UVC groups, including the genes *recA* (C789_RS19850) and *mutM* (C789_RS06635) for DNA repair, whereas the other half were downregulated on the 2nd day. This indicates that these genes play limited direct antioxidant roles, which might be complemented by increasing phycocyanin (PC) synthesis (Supplementary Material Fig. S18). On the 10th day, the expression profiles of genes were similar among all groups, except genes *nth* (C789_RS18080), *gyrB* (C789_RS07200), and *xth* (C789_RS09845) (Supplementary Material Fig. S15b). These three genes are associated with DNA repair resulting from oxidative stress [66–69]. They were all upregulated in the mono UVC and UVA/UVC groups at [1.5, 0.085] and [7.5, 0.085]. In particular, genes *nth* and *xth* were the most upregulated in the UVA/UVC group at [1.5, 0.085] (Supplementary Material Table S12). In addition, GSH levels increased after the 5th day, in a bidirectional pattern, at both molecular and transcriptional levels (Supplementary Material Fig. S19).

As mentioned above, UV irradiation at both wavelengths led to cellular DNA damage, in response to which SOS response genes for DNA damage repair were soon activated (Supplementary Material Fig. S20a, Table S13). Gene *lexA* (C789_RS06150, a transcriptional repressor of SOS response) was downregulated in the mono UVA group at [7.5, 0] on the 2nd day, resulting in the upregulation of most SOS genes. This gene was consistently downregulated in the mono UVC group [0, 0.085] and all the UVA/UVC groups on the 2nd day, combined with the significant upregulation of *recA* (C789_RS19850), resulting in *uvrC* (C789_RS05200) upregulation, which is responsible for the incision of DNA lesions. On the 10th day, the gene *lexA* was the most upregulated in the UVA/UVC groups at [7.5, 0.085] and [14.7, 0.085] (Supplementary Material Fig. S20b), corresponding to the most downregulated SOS genes (Supplementary Material Fig. S20a), including the gene *recA* (Supplementary Material Fig. S20c).

The DNA damage of *M. aeruginosa* cells after UV irradiation was also sensed by the *mazEF* system (Supplementary Material Fig. S21, Table S14). In the mono UVA group [7.5, 0], upregulation patterns of gene *relA* (C789_RS12140, encodes the suppressor of gene *mazE* C789_RS12575), *clp* genes (encodes the suppressor of antitoxin MazE, including *clpP*, C789_RS16245; *clpP*, C789_RS12675; *clpX*, C789_RS12680), gene *mazF* (C789_RS15870) and downregulation of gene *mazE* (C789_RS12575) were recorded on the 2nd day, indicating the activation of the mazF toxin in cells by mono UVA exposure (Supplementary Material Fig. S21) [70]. Nevertheless, most *mazEF* system genes were downregulated in the mono UVC group and all the UVA/UVC groups on the 2nd day. On the 10th day, most genes encoding Clp proteases (genes *clpP*, C789_RS16245; *clpP*, C789_RS07145; and *clpX*, C789_RS12680) were upregulated in the mono UVC group and all the UVA/UVC groups. In addition, both gene *mazF* and gene *mazG* (C789_RS18945), which are responsible for the activation of RCD, were the most upregulated in the UVA/UVC group at [1.5, 0.085] (Fig. 4e; Supplementary Material Fig. S21, Table S14). By contrast, these two genes were downregulated in the UVA/UVC group at [14.7, 0.085], and gene *mazF* was downregulated in the mono UVC group at [0, 0.085] and UVA/UVC group at [7.5, 0.085] (Supplementary Material Fig. S21a). All the above results indicated a shift from ALD on the 2nd day to *mazEF* stress on the 10th day, which was the most activated and initiated RCD in the UVA/UVC group at [1.5, 0.085].

Synergistic damage to the whole photosynthetic ETC by the UVA and UVC combination, together with other mechanisms that will be discussed below, led to the bidirectional impacts of UVA pre-irradiation on UVC-induced intracellular oxidative burst and finally gave rise to divergent cell fates of *M. aeruginosa* cells dependent on *mazEF* stress (Supplementary Material Fig. S22). The highest level of DNA fragmentation (Fig. 4d), significant upregulation of gene *mazF* (Fig. 4e; Supplementary Material Fig. S21, Table S14), and the most damaged cell structure (Supplementary Material Figs. S7 and S8) were observed in the UVA/UVC group at [1.5, 0.085] on the 10th day, indicating the most vital cell death in this group. By contrast, lower DNA fragmentation levels and the downregulation of some *mazEF* genes were recorded in the UVA/UVC groups at [7.5, 0.085] and at [14.7, 0.085] compared with the UVC group at [0, 0.085], suggesting that higher UVA dosages alleviated cell death with more effective DNA repair.

3.4. Divergent mechanisms of UVA and UVC impacts on *M. aeruginosa*

This study illustrated the divergent influences of mono UVA and UVC irradiation on *M. aeruginosa* FACHB905 regarding photosynthetic apparatuses and the DNA damage response. UVA and UVC induced significant upregulation of 381 and 961 genes and downregulation of 494 and 1,274, respectively (Fig. 5a; Supplementary Material Fig. S23). Among these DEGs, 35% and 75% were specific to UVA and UVC irradiation, respectively (Fig. 5a). The principal component analysis results suggested that UVA and UVC differentially impacted *M. aeruginosa* cells (Fig. 5b). GO enrichment analysis (Supplementary Material Fig. S10b) combined with the results of PHYTO-PAM (Fig. 3d; Supplementary Material Fig. S11a), Dual-PAM (Fig. 3b and c), and oxygen evolution tests (Fig. 3a) confirmed that UVA and UVC independently damaged PSI and PSII, respectively. All the PSI reaction center genes were downregulated for the mono UVA group, whereas several PSII genes were upregulated (Supplementary Material Fig. S11b, Table S9) on the 2nd day. However, these genes were all downregulated in the mono UVC group.

Moreover, UVA induced the disassembly of the Fe–S clusters in photosystems. Genes encoding PSI Fe–S center protein (*psaC*, C789_RS03195) (Supplementary Material Table S9) and cytochrome *b*6-f complex Fe–S subunit (C789_RS15225, log2FC = −1.18, FDR = 9.77E−09) were significantly downregulated, contrary to the upregulation of most Fe–S cluster assembly/binding genes in the mono UVA group on the 2nd day, which was not observed in the mono UVC group (Supplementary Material Fig. S24, Table S15). The disassembly of the Fe–S clusters subsequently blocked electron transfer, leading to a 30% decrease in

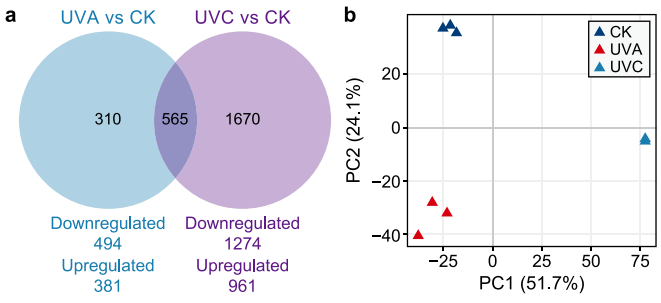

Fig. 5. Comparisons of cellular transcriptomic responses between UVA- and UVC-irradiated *Microcystis aeruginosa* cells. **a**, Venn diagram. **b**, Principal component analysis of gene expression in the control, UVA, and UVC groups. Data presented in Fig. 5 represented the transcriptomic analysis conducted on the 2nd day after UVA and UVC irradiation as cells underwent UV damage, respectively.

the PSI ETC rate (Fig. 3a). Nevertheless, UVC led to a ~75% decrease in the PSII ETC rate (Fig. 3a).

UVA could deactivate several antioxidant enzymes, such as catalase, and thus influence the intracellular H_2O_2 balance [33,37]. GO analysis demonstrated that peroxidase activity in *M. aeruginosa* was significantly influenced (Supplementary Material Fig. S10c), with intracellular H_2O_2 level reaching 1.24-fold of control (Fig. 4b) and upregulation of *oxyR* regulon (Supplementary Material Fig. S25, Table S16) on the 2nd day, especially genes *cmpR* (C789_RS1499) and *grxC* (C789_RS01515) for H_2O_2 detoxification (Supplementary Material Fig. S17). The increased intracellular H_2O_2 could damage Fe–S clusters [71] and react with iron released from disassembled Fe–S clusters to generate hydroxyl radicals (Fig. 4c; Supplementary Material Fig. S22) [72], which is highly reactive to damaged DNA [73].

Ribonucleotide/ribonucleoside metabolism and biosynthesis were significantly influenced in the mono UVA group on the 2nd day (Supplementary Material Fig. S10a), accompanied by the upregulation of most SOS response genes (Supplementary Material Fig. S20), indicating DNA damage can be induced by UVA [74]. Correspondingly, the *mazEF* system was also activated, with most genes encoding Clp proteases and the gene *mazF* upregulated (Supplementary Material Fig. S21). Thus, ALD following the SOS response was postponed [56,57]. However, the lethal effects of *mazF* activation could be effectively counteracted by the mechanism of *trans*-translation with significant upregulation of gene *smpB* (C789_RS22320, Supplementary Material Fig. S26) ($p < 0.05$) [75]. Conversely, a small portion of SOS response genes, including *recA* (C789_RS19850) and *uvrC* (C789_RS05200), were upregulated, with most *mazEF* genes downregulated in the mono UVC group on the 2nd day (Supplementary Material Figs. S20 and S21, Tables S13 and S14). Consequently, divergent regulation patterns of caspase family genes were observed in these two mono UV groups (Supplementary Material Fig. S27a, Table S17).

All the above indicated that UVA and UVC caused damage to the PSI and PSII of *M. aeruginosa*, respectively. In addition, although DNA damage was detected in both groups, differing responses were observed. Bacteriostasis induced in the mono UVA group was indicated by the SOS response and *mazEF* activation [56]. However, a mere SOS response leading to ALD in the mono UVC group characterized by caspase family gene activation was recorded (Supplementary Material Fig. S27), with a 50% increase in DNA fragmentation (Supplementary Material Fig. S16a) and a 7% decrease in cell density (Fig. 2a) on the 2nd day. The differences between the effects of UVA and UVC are summarized in Supplementary Material Fig. S28.

3.5. Mechanisms of the bidirectional impacts of UVA pre-irradiation on UVC-induced suppression

The bidirectional impacts of UVA pre-irradiation on UVC-induced suppression were initiated due to the tradeoff between DNA damage repair provided by UVA and synergistic photosynthetic damage. The low UVA dosage (1.5 J cm^{-2}) aggravated UVC-induced lethality. In contrast, higher UVA dosages (7.5 and 16.54 J cm^{-2}) compromised the algal suppression induced by 0.085 J cm^{-2} UVC in terms of photosynthetic quantum yield (Supplementary Material Fig. S11a), free radicals (Fig. 4a–c), membrane integrity (Fig. 2b), and cell density (Fig. 2a). It was reported that near-ultraviolet radiation (290–400 nm)-induced DNA damage involves several SOS genes, especially gene *recA* [38]. This study observed upregulation of SOS response genes in the mono UVA group at [7.5, 0] on the 2nd day (Supplementary Material Fig. S20). In contrast, the UVC group at [0, 0.085] caused severe DNA damage on the 2nd day. Most SOS genes were downregulated, except for gene *recA* (C789_RS19850) (Fig. 6a). The synergy of damage to photosynthesis outweighed the enhanced repair activity, resulting in the enhanced suppression effects and lysis of viable cells (Fig. 6b).

With increasing UVA dosages, elevated expression levels of most SOS response genes, including gene *recA* (Fig. 6a), were detected. This was the most significant in the UVA/UVC groups at [7.5, 0.085] and [14.7, 0.085], where most SOS genes were upregulated compared with the control. In this study, 7.5 J cm^{-2} UVA alone induced DNA damage, as indicated by GO enrichment analysis (Supplementary Material Fig. S10a), SOS response (Supplementary Material Fig. S20), and the *mazEF* system (Supplementary Material Fig. S21). Nevertheless, negligible impacts on cell growth were observed (Fig. 2a). Consequently, it can be proposed that UVA irradiation at 7.5 J cm^{-2} and above stimulated the biosynthesis of SOS proteins, although insufficient, to repair UVC-induced DNA damage in cells [38]. This was conducive to alleviating the UVC-induced suppression of *M. aeruginosa* and stimulated the growth of viable cells (Fig. 6b).

Different strategies utilized by *M. aeruginosa* to generate ATP revealed the tradeoff between DNA damage repair and photosynthetic damage aggravation, contributing to the bidirectional impacts of UVA pre-irradiation from the perspective of energy acquisition. Because of selective damage to PSI and PSII in *M. aeruginosa*, different partition ratios of linear electron flow (from PSII to PSI) and cyclic electron flow (CEF) (centered around PSI) [76,77] were discovered in *M. aeruginosa* under UV irradiation to generate ATP. UVC exposure induced cells to employ mainly CEF, indicated by hardly influenced PSI activities (Fig. 3a) and the highest upregulation of most *ndh* genes for CEF (Supplementary Material Fig. S29, Table S18). Nevertheless, with the increase in UVA dosages, the upregulation levels of *ndh* genes decreased, suggesting a weakening CEF pathway. As mentioned above, PSI is more susceptible to UVA, whereas PSII is more sensitive to UVC (Supplementary Material Figs. S10b and e; Fig. 3a). This was also indicated by the phenomenon in which higher UVA dosages (7.5 and 14.7 J cm^{-2}) induced higher expression of *psa* genes and lower expression of *psb* genes compared with the mono UVC group on the 10th day (Supplementary Material Fig. S11b). Moreover, an increasing upregulation of genes encoding ATP synthase subunits was detected with increasing UVA dosages to 7.5 and 14.7 J cm^{-2} (Supplementary Material Fig. S12b). Stronger CEF in the UVC group at [0, 0.085] and the higher expression of ATP synthase genes in the UVA/UVC groups at [7.5, 0.085] and [14.7, 0.085], possibly derived from repair of UVC-induced DNA damage, contributed to higher ATP levels in these groups than in the UVA/UVC group at [1.5, 0.085] (Fig. 6c).

Accordingly, the bidirectional impacts of UVA pre-irradiation on UVC-induced suppression were detected in variations of *Y*(II), and thus, the generation of free radicals after the 7th day (Fig. 4a–c; Supplementary Material Fig. S22). It caused DNA oxidative damage indicated by the occurrence of PPBs (Supplementary Material Fig. S7) and upregulation of genes *nth* (C789_RS18080), *gyrB* (C789_RS07200), and *xth* (C789_RS09845), which are responsible for the repair of oxidative DNA damage (Supplementary Material Fig. S15b). This eventually led to differential expression profiles of *mazEF* genes on the 10th day (Fig. 4e; Supplementary Material Figs. S21 and S30).

3.6. The tradeoff roles of UVA pre-irradiation in regulating *M. aeruginosa* cell death modes

This study illustrated the tradeoff roles of UVA pre-irradiation between the repair of UVC-induced DNA damage and the aggravation of photosynthesis damage, leading to divergent cell fates

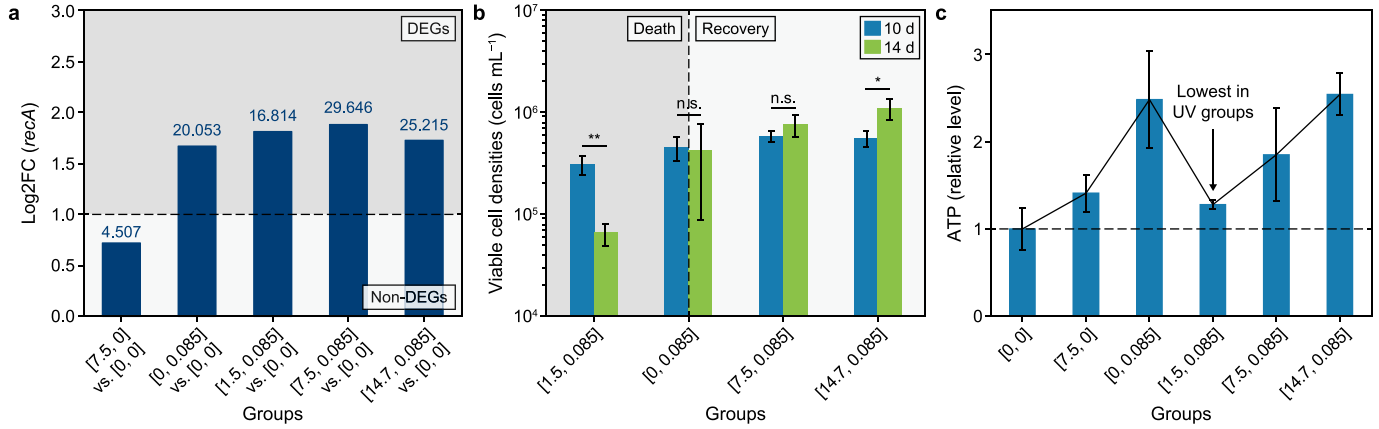

Fig. 6. Mechanisms of bidirectional impacts of UVA pre-irradiation on *Microcystis aeruginosa* cells upon UVC exposure. **a**, Log2FC of the gene *recA* on the 2nd day after UV irradiation. The data above columns represent −log10(FDR) of gene expression changes, and genes with −log10(FDR) values above 1.301 are considered DEGs. **b**, Variations of viable cell densities from the 10th to the 14th day after UV irradiation. **c**, ATP levels in *M. aeruginosa* cells on the 10th day after UV irradiation. UVA pre-irradiation provided RecA repair proteins for UVC-induced damage. Whether the repair kept pace with the damage determined the bidirectional impacts. Asterisks indicate significant differences with * at $p < 0.05$ and ** at $p < 0.01$; n. s. represents not significant. The error bar represents the standard deviation from the three biological replicates.

dependent on UVA dosages. For the samples exposed to UVA pre-irradiation at 1.5 J cm^{-2}, the highest $O_2^{\cdot-}$ and •OH (Fig. 4a–c) were detected and resulted in the highest expression of genes *mazF* (C789_RS15870) and *mazG* (C789_RS15870) (Fig. 4e; Supplementary Material Fig. S21, Table S14). In addition, DNA damage induced the formation of PPBs (Supplementary Material Fig. S7) [78,79], which could activate Clp proteases (Supplementary Material Fig. S21) and cause mazF stress [80]. On the transcriptomic level, the expressions of *clp* genes, including *clpP* (C789_RS16245 and C789_RS01745) and *clpX* (C789_RS12680), were activated in the order of UVA/UVC group at [1.5, 0.085] > mono UVC group > UVA/UVC group at [7.5, 0.085] ≈ UVA/UVC group at [14.7, 0.085]. Thus, microalgal cells in the UVA/UVC group at [1.5, 0.085] experienced the most muscular mazF stress and finally underwent *mazEF*-mediated RCD, as indicated by the highest percentage of cells with permeabilized membranes [57] (Fig. 2b) and lysis of viable cells (Fig. 6b) after the 10th day. This was also the case for cells in the mono UVC group but to a lesser extent. In contrast, the mazF stress levels were insufficient to induce massive cell death in the UVA/UVC groups at [7.5, 0.085] and [14.7, 0.085]. Instead, temporary growth arrest could be detected in these groups, as indicated by the recovery of cell density since the 10th day (Fig. 2a and 6b). These results agree with the microbial dormancy continuum hypothesis [58].

This study proposed the intertwining of *mazEF*-mediated RCD and ALD, first reported in cyanobacterium *M. aeruginosa*. Increases in caspase-3-like enzyme activities indicating ALD (Supplementary Material Fig. S27b) were observed since the 10th day. However, typical hallmarks, such as shrinkage of cells [29] and membrane depolarization [75], were absent in this study. Conversely, insignificant cell size changes (Supplementary Material Figs. S7 and S8) and elevated membrane potential (Supplementary Material Text S2, Fig. S31) were recorded [81]. The increase in membrane potential might result from the activation of CEF (Supplementary Material Fig. S29, Table S18), which is conducive to plastoquinone-mediated proton translocation from chloroplast stroma into the thylakoid lumen [82,83]. Besides, severely compromised membrane integrity was also observed (Fig. 2b). It was once reported that the release of infochemicals accompanied *mazEF*-mediated RCD [84], which was characterized by decreased *recA* mRNA levels (Supplementary Material Fig. S32), suppressed SOS response and ALD, absence of membrane depolarization, and significant loss of cell membrane integrity resulting from DNA damage in *E. coli* [57]. These two intertwined RCD modes were reasoned to determine different survival strategies adopted by prokaryotic cells in response to stress, with ALD acting on individual levels and *mazEF* on population levels [57]. Intertwined RCD modes have also been evidenced in eukaryotic cells [85–87]. Furthermore, a one-to-one correspondence regarding various RCD modes between prokaryotes and eukaryotes has been reported based on endosymbiosis theory [56,88,89]. This study suggests the potential of *mazEF* stress induction in regulating cyanobacterial physiology for HCB management.

4. Conclusions

This study has shed light on the intricate effects of UVA pre-irradiation on the suppression of *Microcystis aeruginosa* growth induced by UVC irradiation. Our findings underscore the bidirectional nature of UVA's impacts, in which low dosages of UVA enhanced UVC's lethal effects, while higher dosages counteracted this suppression by activating DNA repair mechanisms. This study's comprehensive analysis, integrating physiological, molecular, and transcriptomic data, has provided a deeper understanding of the cellular responses to UVA and UVC, particularly regulating cell death pathways. The results indicate that UVA pre-irradiation can modulate the modes of cell death in *M. aeruginosa*, with the most prominent *mazEF*-mediated RCD observed in cells pre-irradiated with 1.5 J cm^{-2} UVA. This RCD is characterized by elevated intracellular ROS and upregulation of genes involved in the *mazEF* pathway. The study suggests that optimizing the balance between UVA and UVC exposure could lead to more effective treatment strategies for managing HCBs, with potential applications in water treatment and environmental management. The insights gained from this study could inform the design of more sustainable and environmentally friendly approaches to managing harmful algal blooms. Future studies should investigate the impacts of natural aquatic conditions, such as temperature, pH, and nutrient availability, on the synergistic effects of UVA and UVC.

Data availability

Data are available on request to authors.

CRediT authorship contribution statement

Yinjie Zhu: Methodology, Formal Analysis, Investigation, Data Curation, Writing - Original Draft, Visualization. **Jian Ding:** Conceptualization, Methodology, Formal Analysis, Investigation, Writing - Review & Editing. **Xiaoxiong Wang:** Writing - Review & Editing. **Xuejian Wang:** Investigation, Writing - Review & Editing. **Huansheng Cao:** Methodology, Software, Data Curation. **Fei Teng:** Conceptualization, Methodology. **Shishi Yao:** Investigation. **Zhiru Lin:** Investigation. **Yuelu Jiang:** Resources. **Yi Tao:** Conceptualization, Writing - Review & Editing, Supervision, Project Administration, Funding Acquisition.

Declaration of competing interest

The authors declare that they have no known competing financial interests or personal relationships that could have appeared to influence the work reported in this paper.

Acknowledgements

This work was supported by the National Natural Science Foundation of China (52070117), Research Projects from Shenzhen Municipal Science and Technology Innovation Council (WDZC20200819163549002, JCYJ20200109142822787), Guangdong Higher Education Institutions Innovative Research Team of Urban Water Cycle and Ecological Safety, China (2023KCXTD053), Shenzhen Science and Technology Program, China (ZDSYS20220606100806014).

Appendix A. Supplementary data

Supplementary data to this article can be found online at https://doi.org/10.1016/j.ese.2024.100455.

References

[1] R. Dai, Y. Xiong, Y. Ma, T. Tang, Algae removal performance of UV-radiation-enhanced coagulation for two representative algal species, Sci. Total Environ. 745 (2020) 141013.
[2] A.A. Santos, D.O. Guedes, M.U.G. Barros, S. Oliveira, A.B.F. Pacheco, S.M.F.O. Azevedo, V.F. Magalhães, C.J. Pestana, C. Edwards, L.A. Lawton, J. Capelo-Neto, Effect of hydrogen peroxide on natural phytoplankton and bacterioplankton in a drinking water reservoir: mesocosm-scale study, Water Res. 197 (2021) 117069.
[3] X. Zhu, G. Dao, Y. Tao, X. Zhan, H. Hu, A review on control of harmful algal blooms by plant-derived allelochemicals, J. Hazard Mater. 401 (2021) 123403.
[4] Y. Tao, D. Hou, T. Zhou, H. Cao, W. Zhang, X. Wang, UV-C suppression on hazardous metabolites in *Microcystis aeruginosa*: unsynchronized production of microcystins and odorous compounds at population and single-cell level, J. Hazard Mater. 359 (2018) 281–289.
[5] B. Žegura, A. Štraser, M. Filipič, Genotoxicity and potential carcinogenicity of cyanobacterial toxins-A review, Rev. Mutat. Res. 727 (2011) 16–41.
[6] M. Su, Y. Zhu, Z. Jia, T. Liu, J. Yu, M. Burch, M. Yang, Identification of MIB producers and odor risk assessment using routine data: a case study of an estuary drinking water reservoir, Water Res. 192 (2021) 116848.
[7] S. Suurnäkki, G.V. Gomez-Saez, A. Rantala-Ylinen, J. Jokela, D.P. Fewer, K. Sivonen, Identification of geosmin and 2-methylisoborneol in cyanobacteria and molecular detection methods for the producers of these compounds, Water Res. 68 (2015) 56–66.
[8] S.H. Te, B.F. Tan, J.R. Thompson, K.Y. Gin, Relationship of microbiota and cyanobacterial secondary metabolites in *planktothricoides*-dominated bloom, Environ. Sci. Technol. 51 (2017) 4199–4209.
[9] X. Wang, Y. Zhu, D. Hou, F. Teng, Z. Cai, Y. Tao, Production of β-cyclocitral and its precursor β-carotene in *Microcystis aeruginosa*: variation at population and single-cell levels, Toxins 14 (2022) 201.
[10] A.M. Dietrich, G.A. Burlingame, Critical review and rethinking of USEPA secondary standards for maintaining organoleptic quality of drinking water, Environ. Sci. Technol. 49 (2015) 708–720.
[11] Y. Dai, S. Yang, D. Zhao, C. Hu, W. Xu, D.M. Anderson, Y. Li, X. Song, D.G. Boyce, L. Gibson, C. Zheng, L. Feng, Coastal phytoplankton blooms expand and intensify in the 21st century, Nature 615 (2023) 280–284.
[12] H. Sakai, K. Oguma, H. Katayama, S. Ohgaki, Effects of low- or medium-pressure UV on the release of intracellular microcystin, Water Res. 41 (2007) 3458–3464.
[13] H. Sakai, K. Oguma, H. Katayama, S. Ohgaki, Effects of low- or medium-pressure ultraviolet lamp irradiation on *Microcystis aeruginosa* and *Anabaena variabilis*, Water Res. 41 (2007) 11–18.
[14] C. Ahn, M. Park, S. Joung, H. Kim, K. Jang, H. Ou, Growth inhibition of cyanobacteria by ultrasonic radiation: laboratory and enclosure studies, Environ. Sci. Technol. 37 (2003) 3031–3037.
[15] M. Yilimulati, J. Jin, X. Wang, X. Wang, D. Shevela, B. Wu, K. Wang, L. Zhou, Y. Jia, B. Pan, G. Govindjee, S. Zhang, Regulation of photosynthesis in bloom-forming cyanobacteria with the simplest β-diketone, Environ. Sci. Technol. 55 (2021) 14173–14184.
[16] M. Yilimulati, L. Zhou, D. Shevela, S. Zhang, Acetylacetone interferes with carbon and nitrogen metabolisms of *Microcystis aeruginosa* by cutting off the electron flow to ferredoxin, Environ. Sci. Technol. 56 (2022) 9683–9692.
[17] C. Zhang, G. Zhang, J. Jin, H. Zheng, Z. Zhou, S. Zhang, Selenite-catalyzed reaction between benzoquinone and acetylacetone deciphered the enhanced inhibition on *Microcystis aeruginosa* growth, Environ. Sci. Technol. 57 (2023) 6188–6195.
[18] D.J. Barrinton, A. Ghadouani, Application of hydrogen peroxide for the removal of toxic cyanobacteria and other phytoplankton from wastewater, Environ. Sci. Technol. 42 (2008) 8916–8921.
[19] X. Huo, D. Chang, J. Tseng, M.D. Burch, T. Lin, Exposure of *Microcystis aeruginosa* to hydrogen peroxide under light: kinetic modeling of cell rupture and simultaneous microcystin degradation, Environ. Sci. Technol. 49 (2015) 5502–5510.
[20] C.J. Pestana, A.A. Santos, J. Capelo-Neto, V.M.M. Melo, K.C. Reis, S. Oliveira, R. Rogers, A.B.F. Pacheco, J. Hui, N.C. Skillen, M.U.G. Barros, C. Edwards, S.M.F.O. Azevedo, P.K.J. Robertson, J.T.S. Irvine, L.A. Lawton, Suppressing cyanobacterial dominance by UV-LED TiO_2-photocatalysis in a drinking water reservoir: a mesocosm study, Water Res. 226 (2022) 119299.
[21] K.V. Ajayan, P.J. Chaithra, K. Sridharan, P. Sruthi, E. Harikrishnan, C.C. Harilal, Synergistic influence of iodine and hydrogen peroxide towards the degradation of harmful algal bloom of *Microcystis aeruginosa*, Environ. Res. 237 (2023) 116926.
[22] L. Cao, J. Wang, Z. Wang, S. Yu, Y. Cheng, J. Ma, P. Xie, Inactivation of *Microcystis Aeruginosa* by peracetic acid combined with ultraviolet: performance and characteristics, Water Res. 208 (2022) 117847.
[23] J. Zheng, F. Teng, T. Zhou, H. Cao, X. Wang, Y. Zhu, Y. Tao, Enhanced suppression effects on *Microcystis aeruginosa* by combining hydrogen peroxide and intermittent UVC irradiation: the importance of triggering advanced oxidation process within cells, J. Hazard Mater. 463 (2024) 132826.
[24] S. Li, Y. Tao, G. Dao, H. Hu, Synergetic suppression effects upon the combination of UV-C irradiation and berberine on *Microcystis aeruginosa* and *Scenedesmus obliquus* in reclaimed water: effectiveness and mechanisms, Sci. Total Environ. 744 (2020) 140937.
[25] L. Urban, S.D. Chabane, B. Orsal, M. Lopes, R. Miranda, J. Aarrouf, UV-C light and pulsed light as alternatives to chemical and biological elicitors for stimulating plant natural defenses against fungal diseases, Sci. Hortic. 235 (2018) 452–459.
[26] Y. Tao, X. Mao, J. Hu, H.O.L. Mok, L. Wang, D.W.T. Au, J. Zhu, X. Zhang, Mechanisms of photosynthetic inactivation on growth suppression of *Microcystis aeruginosa* under UV-C stress, Chemosphere 93 (2013) 637–644.
[27] P.M. Mullineaux, M. Exposito-Rodriguez, P.P. Laissue, N. Smirnoff, ROS-dependent signalling pathways in plants and algae exposed to high light: comparisons with other eukaryotes, Free Radical Biol. Med. 122 (2018) 52–64.
[28] T. Phukan, M.B. Syiem, Modulation of oxidant and antioxidant homeostasis in the cyanobacterium *Nostoc muscorum* Meg1 under UV-C radiation stress, Aquat. Toxicol. 213 (2019) 105228.
[29] T. Zhou, H. Cao, J. Zheng, F. Teng, X. Wang, K. Lou, X. Zhang, Y. Tao, Suppression of water-bloom cyanobacterium *Microcystis aeruginosa* by algaecide hydrogen peroxide maximized through programmed cell death, J. Hazard Mater. 393 (2020) 122394.
[30] M. Wang, Y. Zhan, C. Chen, M. Chen, J. Zhu, X. Jiang, Y. Yang, X. Lv, P. Yin, W. Zhang, L. Yang, Amplified cyanobacterial bloom is derived by polyphosphate accumulation triggered by ultraviolet light, Water Res. 222 (2022) 118837.
[31] A. Hamamoto, M. Mori, A. Takahashi, M. Nakano, N. Wakikawa, M. Akutagawa, T. Ikehara, Y. Nakaya, Y. Kinouchi, New water disinfection system using UVA light-emitting diodes, J. Appl. Microbiol. 103 (2007) 2291–2298.
[32] J. Li, K. Hirota, H. Yumoto, T. Matsuo, Y. Miyake, T. Ichikawa, Enhanced germicidal effects of pulsed UV-LED irradiation on biofilms, J. Appl. Microbiol. 109 (2010) 2183–2190.
[33] L. Feng, C. Peillex-Delphe, C. Lü, D. Wang, S. Giannakis, C. Pulgarin, Employing bacterial mutations for the elucidation of photo-Fenton disinfection: focus on the intracellular and extracellular inactivation mechanisms induced by UVA and H_2O_2, Water Res. 182 (2020) 116049.
[34] K. Song, M. Mohseni, F. Taghipour, Mechanisms investigation on bacterial inactivation through combinations of UV wavelengths, Water Res. 163 (2019) 114875.
[35] J. Cadet, T. Douki, J.L. Ravanat, Oxidatively generated damage to cellular DNA by UVB and UVA radiation, Photochem. Photobiol. 91 (2015) 140–155.
[36] J.D. Hoerter, A.A. Arnold, D.A. Kuczynska, A. Shibuya, C.S. Ward, M.G. Sauer, A. Gizachew, T.M. Hotchkiss, T.J. Fleming, S. Johnson, Effects of sublethal UVA irradiation on activity levels of oxidative defense enzymes and protein

oxidation in *Escherichia coli*, J. Photochem. Photobiol. B Biol. 81 (2005) 171–180.
[37] S. Giannakis, A. Gupta, C. Pulgarin, J. Imlay, Identifying the mediators of intracellular *E. coli* inactivation under UVA light: the (photo) Fenton process and singlet oxygen, Water Res. 221 (2022) 118740.
[38] A. Eisenstark, Bacterial genes involved in response to near-ultraviolet radiation, Adv. Genet. 26 (1989) 99–147.
[39] A.C. Chevremont, A.M. Farnet, B. Coulomb, J.L. Boudenne, Effect of coupled UV-A and UV-C LEDs on both microbiological and chemical pollution of urban wastewaters, Sci. Total Environ. 426 (2012) 304–310.
[40] A.C. Chevremont, A.M. Farnet, M. Sergent, B. Coulomb, J.L. Boudenne, Multivariate optimization of fecal bioindicator inactivation by coupling UV-A and UV-C LEDs, Desalination 285 (2012) 219–225.
[41] K. Song, F. Taghipour, M. Mohseni, Microorganisms inactivation by wavelength combinations of ultraviolet light-emitting diodes (UV-LEDs), Sci. Total Environ. 665 (2019) 1103–1110.
[42] Y. Xiao, X.N. Chu, M. He, X.C. Liu, J.Y. Hu, Impact of UVA pre-radiation on UVC disinfection performance: inactivation, repair and mechanism study, Water Res. 141 (2018) 279–288.
[43] R. Chandra, P. Das, G. Vishal, S. Nagra, Factors affecting the induction of UV protectant and lipid productivity in *Lyngbya* for sequential biorefinery product recovery, Bioresour. Technol. 278 (2019) 303–310.
[44] R. Chandra, F.P. Pons-Faudoa, R.P. Saldívar, B.E. Rittmann, Effect of ultra-violet exposure on production of mycosporine-like amino acids and lipids by *Lyngbya purpurem*, Biomass Bioenergy 134 (2020) 105475.
[45] J.J. Huang, P.C. Cheung, Enhancement of polyunsaturated fatty acids and total carotenoid production in microalgae by ultraviolet band A (UVA, 365 nm) radiation, J. Agric. Food Chem. 59 (2011) 4629–4636.
[46] A. Salguero, R. León, A. Mariotti, B. De La Morena, J.M. Vega, C. Vílchez, UV-A mediated induction of carotenoid accumulation in *Dunaliella bardawil* with retention of cell viability, Appl. Microbiol. Biotechnol. 66 (2005) 506–511.
[47] C. Holohan, S.V. Schaeybroeck, D.B. Longley, P.G. Johnston, Cancer drug resistance: an evolving paradigm, Nat. Rev. Cancer 13 (2013) 714–726.
[48] X. Cheng, J.E. Ferrell, Apoptosis propagates through the cytoplasm as trigger waves, Science 361 (2018) 607–612.
[49] K. Newton, D.L. Dugger, K.E. Wickliffe, N. Kapoor, M.C. De Almagro, D. Vucic, L. Komuves, R.E. Ferrando, D.M. French, J. Webster, M. Roose-Girma, S. Warming, V.M. Dixit, Activity of protein kinase RIPK3 determines whether cells die by necroptosis or apoptosis, Science 343 (2014) 1357–1360.
[50] Z. Zhou, H. He, K. Wang, X. Shi, Y. Wang, Y. Su, Y. Wang, D. Li, W. Liu, Y. Zhang, L. Shen, W. Han, L. Shen, J. Ding, F. Shao, Granzyme A from cytotoxic lymphocytes cleaves GSDMB to trigger pyroptosis in target cells, Science 368 (2020) eaaz7548。.
[51] J. Nassour, R. Radford, A. Correia, J.M. Fusté, B. Schoell, A. Jauch, R.J. Shaw, J. Karlseder, Autophagic cell death restricts chromosomal instability during replicative crisis, Nature 565 (2019) 659–663.
[52] D.C. Sigee, A. Selwyn, P. Gallois, A.P. Dean, Patterns of cell death in freshwater colonial cyanobacteria during the late summer bloom, Phycologia 46 (2007) 284–292.
[53] H. Lee, D.G. Lee, Programmed cell death in bacterial community: mechanisms of action, causes and consequences, J. Microbiol. Biotechnol. 29 (2019) 1014–1021.
[54] S. Amitai, Y. Yassin, H. Engelberg-Kulka, MazF-mediated cell death in *Escherichia coli*: a point of no return, J. Bacteriol. 186 (2004) 8295–8300.
[55] R. Hazan, B. Sat, H. Engelberg-Kulka, *Escherichia coli mazEF*-mediated cell death is triggered by various stressful conditions, J. Bacteriol. 186 (2004) 3663–3669.
[56] K.W. Bayles, Bacterial programmed cell death: making sense of a paradox, Nat. Rev. Microbiol. 12 (2014) 63–69.
[57] A. Erental, I. Sharon, H. Engelberg-Kulka, Two programmed cell death systems in *Escherichia coli*: an apoptotic-like death is inhibited by the *mazEF*-mediated death pathway, PLoS Biol. 10 (2013) e1001281.
[58] M. Ayrapetyan, T.C. Williams, J.D. Oliver, Bridging the gap between viable but non-culturable and antibiotic persistent bacteria, Trends Microbiol. 23 (2015) 7–13.
[59] D. Wen, D. Chen, Y. Jiang, Synergistic algicidal effects of combined UV-LED/chlorine treatments on *Tetraselmis* sp.: optimization and mode-of-action, Chem. Eng. J. 422 (2021) 130043.
[60] Y. Qiao, D. Chen, D. Wen, Use of coupled wavelength ultraviolet light-emitting diodes for inactivation of bacteria in subsea oil-field injection water, Sci. Total Environ. 640–641 (2018) 757–763.
[61] J.R. Bolton, K.G. Linden, Standardization of methods for fluence (UV dose) determination in bench-scale UV experiments, J. Environ. Eng. 129 (2003) 209–215.
[62] R. Yin, Y. Zhang, Y. Wang, J. Zhao, C. Shang, Far-UVC photolysis of peroxydisulfate for micropollutant degradation in water, Environ. Sci. Technol. 58 (2024) 6030–6038.
[63] Z. Chen, P. Juneau, B. Qiu, Effects of three pesticides on the growth, photosynthesis and photoinhibition of the edible cyanobacterium Ge-Xian-Mi (*Nostoc*), Aquat. Toxicol. 81 (2007) 256–265.
[64] J. Zhu, B. Liu, J. Wang, Y. Gao, Z. Wu, Study on the mechanism of allelopathic influence on cyanobacteria and chlorophytes by submerged macrophyte (*Myriophyllum spicatum*) and its secretion, Aquat. Toxicol. 98 (2010) 196–203.
[65] H. Wang, G. Qu, Y. Gan, Z. Zhang, R. Li, T. Wang, Elimination of *Microcystis aeruginosa* in water via dielectric barrier discharge plasma: efficacy, mechanism and toxin release, J. Hazard Mater. 422 (2022) 126956.
[66] N. Moolla, V.J. Goosens, B.D. Kana, B.G. Gordhan, The contribution of Nth and Nei DNA glycosylases to mutagenesis in *Mycobacterium smegmatis*, DNA Repair 13 (2014) 32–41.
[67] R.P. Cunningham, B. Weiss, Endonuclease III (nth) mutants of *Escherichia coli*, Proc. Natl. Acad. Sci. USA 82 (1985) 474–478.
[68] A.K. Ujaoney, M.K. Padwal, B. Basu, Proteome dynamics during post-desiccation recovery reveal convergence of desiccation and gamma radiation stress response pathways in *Deinococcus radiodurans*, Biochim. Biophys. Acta-Proteins Proteom. 1865 (2017) 1215–1226.
[69] T.C.V. Wang, H.Y. Chang, Effect of *rec* mutations on viability and processing of DNA damaged by methylmethane sulfonate in *xth nth nfo* cells of *Escherichia coli*, Biochem. Biophys. Res. Commun. 180 (1991) 774–781.
[70] E. Aizenman, H. Engelberg-Kulka, G. Glaser, An *Escherichia coli* chromosomal "addiction module" regulated by 3',5'-bispyrophosphate: a model for programmed bacterial cell death, Proc. Natl. Acad. Sci. USA 93 (1996) 6059–6063.
[71] S. Jang, J.A. Imlay, Micromolar intracellular hydrogen peroxide disrupts metabolism by damaging iron-sulfur enzymes, J. Biol. Chem. 282 (2007) 929–937.
[72] H. Cao, D. Wei, Y. Yang, Y. Shang, G. Li, Y. Zhou, Q. Ma, Y. Xu, Systems-level understanding of ethanol-induced stresses and adaptation in *E. coli*, Sci. Rep. 7 (2017) 44150.
[73] D.J. Dwyer, D.M. Camacho, M.A. Kohanski, J.M. Callura, J.J. Collins, Antibiotic-induced bacterial cell death exhibits physiological and biochemical hallmarks of apoptosis, Mol. Cell 46 (2012) 561–572.
[74] S.P. Kidambi, M.G. Booth, T.A. Kokjohn, R.V. Miller, *recA*-dependence of the response of *Pseudomonas aeruginosa* to UVA and UVB irradiation, Microbiology 142 (1996) 1033–1040.
[75] A.M. Hall, B. Gollan, S. Helaine, Toxin-antitoxin systems: reversible toxicity, Curr. Opin. Microbiol. 36 (2017) 102–110.
[76] Y. Munekage, M. Hashimoto, C. Miyake, K.I. Tomizawa, T. Endo, M. Tasaka, T. Shikanai, Cyclic electron flow around photosystem I is essential for photosynthesis, Nature 429 (2004) 579–582.
[77] Y. Zheng, C. Xue, H. Chen, C. He, Q. Wang, Low-Temperature adaptation of the snow alga *Chlamydomonas nivalis* is associated with the photosynthetic system regulatory process, Front. Microbiol. 11 (2020) 123.
[78] P.L. Foster, Stress-induced mutagenesis in bacteria, Crit. Rev. Biochem. Mol. Biol. 42 (2007) 373–397.
[79] K. Tsutsumi, M. Munekata, T. Shiba, Involvement of inorganic polyphosphate in expression of SOS genes, Biochim. Biophys. Acta Gene Struct. Expr. 1493 (2000) 73–81.
[80] Y. Cai, J. Liu, G. Li, P.K. Wong, T. An, Formation mechanisms of viable but nonculturable bacteria through induction by light-based disinfection and their antibiotic resistance gene transfer risk: a review, Crit. Rev. Environ. Sci. Technol. 52 (2022) 3651–3688.
[81] S. Li, Y. Tao, G.H. Dao, H.Y. Hu, Synergetic suppression effects upon the combination of UV-C irradiation and berberine on *Microcystis aeruginosa* and *Scenedesmus obliquus* in reclaimed water: effectiveness and mechanisms, Sci. Total Environ. 744 (2020) 140937.
[82] J. Steinbeck, I.L. Ross, R. Rothnagel, P. Gäbelein, S. Schulze, N. Giles, R. Ali, R. Drysdale, E. Sierecki, Y. Gambin, H. Stahlberg, Y. Takahashi, M. Hippler, B. Hankamer, Structure of a PSI-LHCI-cyt b_6f supercomplex in *Chlamydomonas reinhardtii* promoting cyclic electron flow under anaerobic conditions, Proc. Natl. Acad. Sci. USA 115 (2018) 10517–10522.
[83] M.E. Christensen, E.S. Jansen, W. Sanchez, N.J. Waterhouse, Flow cytometry based assays for the measurement of apoptosis-associated mitochondrial membrane depolarisation and cytochrome c release, Methods 61 (2013) 138–145.
[84] I. Kolodkin-Gal, R. Hazan, A. Gaathon, S. Carmeli, H. Engelberg-Kulka, A linear pentapeptide is a quorum-sensing factor required for *mazEF*-mediated cell death in *Escherichia coli*, Science 318 (2007) 652–655.
[85] M.J. Abedin, D. Wang, M.A. McDonnell, U. Lehmann, A. Kelekar, Autophagy delays apoptotic death in breast cancer cells following DNA damage, Cell Death Differ. 14 (2007) 500–510.
[86] B. Chen, Y. Yan, Y. Yang, G. Cao, X. Wang, Y. Wang, F. Wan, Q. Yin, Z. Wang, Y. Li, L. Wang, B. Xu, F. You, Q. Zhang, Y. Wang, A pyroptosis nanotuner for cancer therapy, Nat. Nanotechnol. 17 (2022) 788–798.
[87] M.L. Goodall, B.E. Fitzwalter, S. Zahedi, M. Wu, D. Rodriguez, J.M. Mulcahy-Levy, D.R. Green, M. Morgan, S.D. Cramer, A. Thorburn, The autophagy machinery controls cell death switching between apoptosis and necroptosis, Dev. Cell 37 (2016) 337–349.
[88] T.M. Embley, W. Martin, Eukaryotic evolution, changes and challenges, Nature 440 (2006) 623–630.
[89] S.D. Dyall, M.T. Brown, P.J. Johnson, Ancient invasions: from endosymbionts to Organelles, Science 304 (2004) 253–257.